Comparison of experiment and theory for superelastic electron-collision studies from laser-aligned magnesium

Journal Item

Comparison of experiment and theory for superelastic electron-collision studies from laser-aligned magnesium

James Pursehouse,[1] Chris Bostock,[2] Kate Nixon,[3] Matthew Harvey,[1] Dmitry V. Fursa,[2] Igor Bray,[2] and Andrew James Murray[1,*]

[1]*Photon Science Institute, School of Physics & Astronomy, University of Manchester, Manchester M13 9PL, United Kingdom*

[2]*Curtin Institute of Computation and Department of Physics and Astronomy, Curtin University, Kent Street, Bentley, Perth, Western Australia 6102, Australia*

[3]*School of Sciences, University of Wolverhampton, Wulfruna Street, Wolverhampton WV1 1LY, United Kingdom*

(Received 2 April 2018; published 9 August 2018)

A combined experimental and theoretical study of superelastic electron collisions from laser-aligned magnesium atoms for a range of collision energies from 35 to 55 eV is presented. ^{24}Mg atoms were excited from the $3\,^1S_0$ ground state to the $3\,^1P_1$ excited state using continuous-wave linearly polarized laser radiation at ∼285 nm. Electrons of well-defined energy $E_{\rm inc}$ then deexcited the targets, and the superelastically scattered electrons emerging from the collision were detected as a function of scattering angle and laser polarization. Results for alignment of the target by the electron beam are presented for a range of scattering angles, for outgoing energies from $E_{\rm out} = 35$ to 55 eV. The agreement between the measurements and the results of the convergent close-coupling theory are encouraging, but some discrepancies remain.

DOI: 10.1103/PhysRevA.98.022702

I. INTRODUCTION

In two visionary papers published in 1969, Bederson [1,2] introduced the concept of a "perfect scattering experiment," one that is able to measure all aspects of the corresponding theoretically determined scattering amplitudes that describe the interaction. Though the scattering amplitudes are complex in nature (carrying both amplitude and phase information), various experimental methods have the capacity to determine both their real and imaginary components. Despite the subsequent enormous experimental effort in this direction, Bederson's vision is yet to be realized fully in any single experiment. Nevertheless, experimental techniques which are referred to as "coincidence measurements" or "superelastic measurements" have made great progress in this regard.

Extraction of the scattering amplitudes that describe electron excitation of an atom normally requires the scattered electron to be detected in coincidence with a photon emitted when the target relaxes to a lower state [3]. These measurements are difficult due to the low probability of coincidence detection, and so often only produce data at small scattering angles, where this probability is highest. The electron-photon coincidence technique has been used to study collisions with different atomic targets, both experimentally and theoretically. These include the lighter targets hydrogen [4–6], helium [7,8], and magnesium [9,10]; intermediate targets including calcium [11–16], neon [17–19], and zinc [20–23]; and heavier targets including cadmium [24–26], lead [27], and mercury [28–33].

An alternative method to coincidence studies is the *superelastic* scattering technique, as adopted here. This method is effectively the time reversal of the coincidence method, and so produces equivalent information about electron-impact excitation as obtained from coincidence studies. In superelastic scattering measurements the atom is first excited by laser radiation with the same energy as the detected photon in coincidence studies. Electrons with well-defined energy $E_{\rm inc}$ are directed at the laser-excited target, so that $E_{\rm inc}$ is equal to that of the *inelastically* scattered electron in a coincidence experiment. Superelastically scattered electrons that gain energy from the reaction are then detected at various scattering angles, for different polarizations of the laser beam. This process is equivalent to measuring the polarization of the emitted photon in coincidence studies. Both types of experiment generate a set of atomic collision parameters (ACPs) [3,34] that define the alignment and orientation of the excited atoms due to the collision; however, the data collection rates are thousands of times faster in superelastic experiments than for coincidence studies. The ACPs are directly related to the real and imaginary parts of the scattering amplitudes, as discussed in Sec. II.

The superelastic scattering technique is, however, limited by the availability of high-intensity, coherent radiation that can be obtained from tunable continuous-wave (cw) lasers. As such, the range of atoms that can be studied is restricted to those that can be excited from their ground state by cw laser radiation. Until recently, tunable lasers could only supply visible and near-infrared light, which limited the range of targets to the alkali atoms sodium [35–37], potassium [38], rubidium [39], lithium [40], and cesium [41], as well as to the heavier targets barium [42–50] and ytterbium [51]. Recent advances in laser developments has extensively opened up this range, since it is now possible to deliver high-intensity, coherent ultraviolet radiation from frequency-doubled cw lasers. This has allowed additional measurements from calcium [52–57] and magnesium, as well as the heavier atomic target silver [58]. It is this work on magnesium that is presented in this paper.

*Andrew.Murray@manchester.ac.uk

Previous experiments to determine the collision parameters for magnesium were carried out by the Newcastle group [9,10] using the coincidence technique, at an incident energy of 20 eV. The data were compared to both convergent close-coupling (CCC) and R-matrix models, with reasonable agreement found between theory and experiment. The data were obtained mostly at small scattering angles, due to the low coincidence yields obtained using this technique. These experiments further could not resolve the different isotopes that are present in Mg, and so assumed that hyperfine contributions from ^{25}Mg were negligible. This is in contrast to the superelastic technique that allows *individual* isotopes to be selected from the atomic ensemble. In coincidence studies the ACPs are derived from the measured Stokes parameters, in contrast to the method adopted here which determines the parameters directly from the data (see Sec. IV below). The uncertainties in the ACPs calculated in [9,10] were hence relatively large, particularly at higher angles. The superelastic technique allows a more extensive angular survey to be conducted to higher precision than is possible using these conventional coincidence methods.

Detailed studies of alkaline-earth atoms are important as these targets have two electrons in the outer valence shell, and so both must be treated on an equal footing to solve the collision dynamics during the interaction. These are in contrast to measurements from alkali targets that only have a single (valence) electron that needs to be considered, thereby simplifying the Coulomb interaction between the incident electron and the target. It is only recently that laser sources have been available to study alkaline-earth targets, and as such the measurements presented here provide information about these more complex collision processes.

This paper is divided into six sections. Following this Introduction the ACPs are described in Sec. II and their relationships to the scattering parameters are given. Section III describes the procedures that were adopted to generate the experimental data. Section IV discusses the convergent close-coupled (CCC) method used to generate the theoretical results, whereas Sec. V compares the results from calculations with experiment, and highlights similarities and differences between them. Conclusions are then drawn from these studies in Sec. VI.

II. DEFINITION OF THE ATOMIC COLLISION PARAMETERS (ACPs)

Excitation of a target atom by an electron beam with energy $E_{\rm inc}$ produces inelastically scattered electrons, whose energy $E_{\rm out}$ is given by the difference between $E_{\rm inc}$ and the target-state excitation energy. The electrons may scatter through different angles θ_e with respect to the incident direction, and the target may relax back to a lower state, releasing a photon whose polarization depends on the alignment and orientation of the excited state. By measuring this polarization in coincidence with the scattered electron, a full determination of the scattering process can be made.

Quantum mechanically, this process is defined by a set of scattering amplitudes that are determined by solving Schrödinger's equation for the interaction. By defining a scattering plane by the momenta of the incident and scattered electrons ($\mathbf{k_{in}}, \mathbf{k_{out}}$), the scattering amplitudes can be calculated in the "natural" frame, where the quantization axis is chosen to be perpendicular to the plane (see Fig. 1) [34]. For excitation of a P state the scattering amplitudes in this frame are given by $f^{\rm Nat}_{\pm1,0}$. Under these conditions the angular momentum transferred to the target during the collision must be perpendicular to the scattering plane, and is given by the atomic collision parameter (ACP) $L_\perp$ so that

$$L_\perp = \frac{\left|f^{\rm Nat}_{+1}\right|^2 - \left|f^{\rm Nat}_{-1}\right|^2}{\left|f^{\rm Nat}_{+1}\right|^2 + \left|f^{\rm Nat}_{-1}\right|^2}. \tag{1}$$

The linear component of the excited-state charge cloud has both magnitude and direction with respect to the incident electron beam, and the ACP *alignment parameters*(P_ℓ, γ) are then given by

$$\begin{aligned} P_\ell &= \frac{\left|f^{\rm Nat}_{+1}\right| \cdot \left|f^{\rm Nat}_{-1}\right|}{\left|f^{\rm Nat}_{+1}\right|^2 + \left|f^{\rm Nat}_{-1}\right|^2}; \\ \gamma &= \frac{1}{2}\left\{\pi \pm \left[\arg\left(f^{\rm Nat}_{+1}\right) - \arg\left(f^{\rm Nat}_{-1}\right)\right]\right\}. \end{aligned} \tag{2}$$

A fourth parameter ρ^A_{00}, related to $f_0^{\rm Nat}$, describes the probability that the electron spin changes during the collision, and should be essentially zero in a nonrelativistic system.

The collision parameters can be determined experimentally by detecting the electron scattered during the reaction, and then measuring the Stokes parameters for the photons emitted perpendicular to the scattering plane in time-correlated coincidence [as in Fig. 1(a)]. The linear Stokes parameters then can be related to the alignment parameters (P_ℓ, γ), and the circular Stokes parameter is directly related to $L_\perp$ [34]. Since the majority of photons from the excited targets are not emitted in the direction of the photomultiplier tube, the accumulation of true coincidence counts is slow, and so these are very time-consuming measurements.

The superelastic scattering scheme adopted here effectively reverses the arrow of time in coincidence studies [see Fig. 1(b)]. In this scheme the atoms are initially excited by laser radiation (1) before electrons are superelastically scattered from the laser-excited targets (2), thereby deexciting them. The rate of superelastically scattered electrons (3) is then measured as a function of the polarization of the laser beam, allowing the ACPs to be determined. Since the laser radiation is always directed in the same direction, superelastic experiments accumulate data many thousands of times faster than is possible using coincidence methods.

In the experiments described here only P_ℓ and γ were determined. The state of magnesium that was measured is the $3\,^1P_1$ state, that was excited from the ground $3\,^1S_0$ state by laser radiation at ∼285.3 nm as shown. The difference in energy between incident and superelastically scattered electrons was therefore 4.35 eV, and so the incident electron beam was set to be 4.35 eV lower in energy than the electron energy selected by the detectors (see Sec. III for details).

III. EXPERIMENTAL PROCEDURE

Figure 2 details the electron spectrometer as viewed from above the scattering plane. The magnesium atomic beam was produced from a custom-built oven positioned in the scattering plane at an angle of ∼50° to the electron gun. Atoms effusing

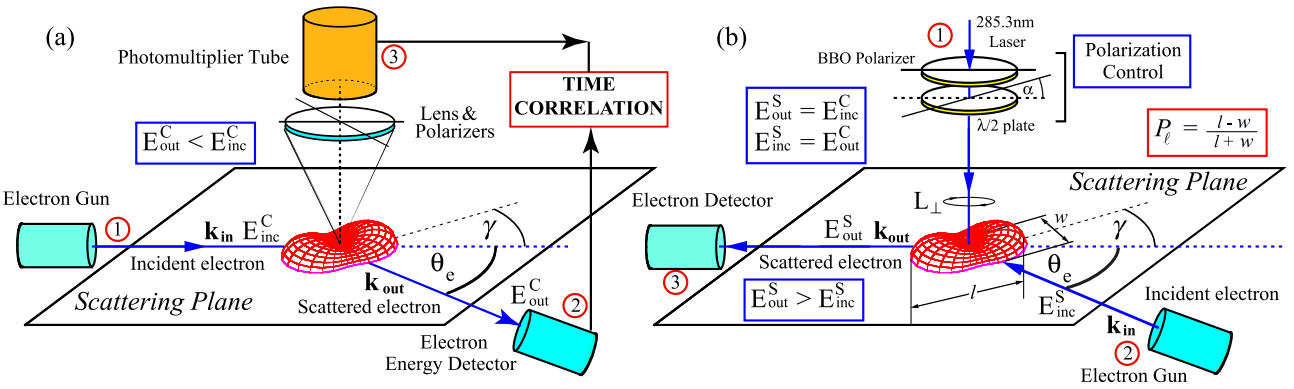

FIG. 1. Determining the charge-cloud alignment and orientation following a collision. (a) In coincidence studies, the incident electron (1) excites the target and is scattered through an angle θ_e to the detector (2). Photons emitted from relaxation of the atom are then detected (3) for different polarizations of the radiation. The scattered electron and correlated photon are then detected in coincidence. (b) In superelastic scattering studies the arrow of time is reversed, so that the state is initially excited by polarized laser radiation (1). An incident electron (2) then *deexcites* the target, the scattered superelastic electrons being detected as a function of laser polarization (3). Alignment of the charge cloud is determined through the parameters P_ℓ and γ, and the angular momentum transferred during the collision is given by $L_\perp$.

from the oven were collected on a cold trap that was maintained at 70 K by directing liquid nitrogen to the cold-trap head. Atoms from the beam were efficiently condensed onto the cold trap, thereby minimizing unwanted coating of components inside the chamber. A gas jet was also installed so that helium could be injected into the interaction region for calibration of the electron energy.

The electron beam was produced from a two-stage gun that has been described in previous work [59]. Electrons that passed undeviated through the interaction region were collected by a Faraday cup as shown. Two electron analyzers collected superelastically scattered electrons, thereby increasing the efficiency of the experiment. The figure shows the scattering angles they could access without colliding with other components in the spectrometer. Analyzer 2 could range from $\theta_2 \sim 35^\circ$ to 80°, whereas analyzer 1 could access from $\theta_1 \sim 25^\circ$ to 35° and could then move from $\theta_1 \sim 70^\circ$ to 145°

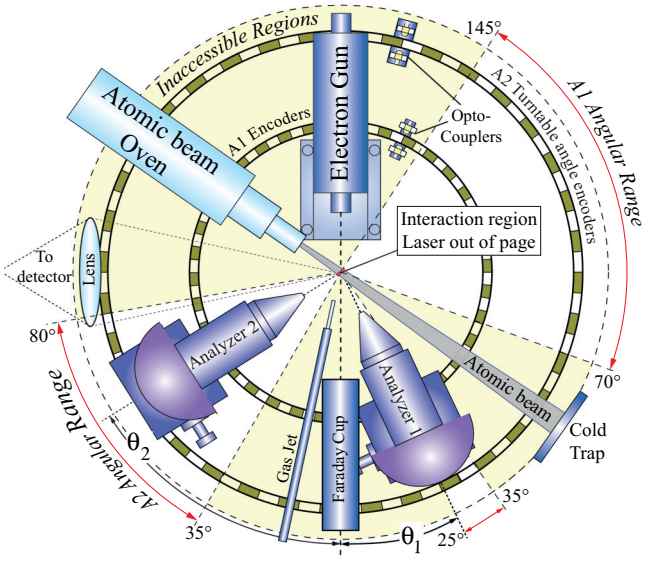

FIG. 2. The experimental apparatus viewed from above the scattering plane. For details see text.

(thereby avoiding the atomic beam). The angle of the analyzers was determined using optocouplers inside the vacuum chamber that measured the position of the encoders that passed through them.

Fluorescence from the laser-atom interaction was monitored using a 50-mm-diameter 70-mm-focal-length fused-silica lens located inside the chamber, which directed light onto an external photodiode. The signal from the photodiode was amplified and sent to a dedicated LABVIEW card that digitized the signal.

The laser system was a Spectra Physics Matisse DX dye-laser pumped by a Millennia 15-W laser. The laser used rhodamine 6G dye, and operated at a wavelength of 570.6 nm. Light from the dye laser was injected into a Spectra Physics WaveTrain frequency doubler that produced coherent radiation at the required wavelength. The dye-laser wavelength was monitored by a HighFinesse WSU wavelength meter that was also used to control the laser so as to produce the required wavelength. Further details on the laser system can be found in [58].

The laser beam was directed from the laser system to the experiment via a collimating lens and mirrors, before entering the chamber through a fused-silica window located on the bottom flange of the chamber. The polarization of the laser was controlled in this final path of the beam by passing the beam through a BBO Glan-laser polarizer and a zero-order half-wave plate. The laser power in the interaction region after passing through the optics was approximately 30 mW, with a beam diameter of around 3 mm. The polarization of the beam in the interaction region was found to be >98% purity, with the half-wave plate defining the polarization vector with respect to the direction of the electron beam. As the wave plate rotated through 360°, the polarization vector of the radiation therefore changed by 720°. The relative alignment angle of the 3^1P_1 state γ then depended on the angle of the wave plate (which defined the direction of polarization of the laser) as well as the angle of the analyzers (since γ is defined with respect to the outgoing electron momentum vector $\mathbf{k_{out}}$ in superelastic scattering experiments).

To produce an atomic beam of sufficient density the oven was operated at a temperature of ∼800 K. Collimation of the atomic beam was carried out using a skimmer and aperture assembly located on the front of the oven, so that the angular spread of the resulting atomic beam was ∼3°. This was confirmed by measuring the diameter of the deposited spot on the cold trap. The size of the atomic beam at the interaction region was hence ∼3 mm in diameter.

The energy of the incident electron beam was calibrated against the known 19.366-eV elastic resonance in helium [60], by injecting helium gas into the interaction region while the oven was operating. The pass energies of the electron analyzers were then set using inelastic scattering measurements from helium targets. Energy calibrations were carried out regularly, so as to allow for any alteration in the contact potential due to deposition of magnesium onto spectrometer components. Only small changes in the contact potential were observed during operation, confirming that the cold trap was effectively trapping atoms from the atomic beam.

The electron analyzers used hemispherical selectors to define the energy of the superelastically scattered electrons, the entrance apertures of the analyzers limiting the angular acceptance to ±3°. Electrons selected by the analyzers were detected by channel electron multipliers (CEMs), whose signals were amplified and counted using high-speed electronics. The detected signals were sent to a LABVIEW PCI 6221 data acquisition card for production of the superelastic data.

The spectrometer was located inside a high-vacuum chamber that was constructed entirely of nonmagnetic 310-grade stainless steel. The chamber was lined internally with μ-metal so as to reduce external magnetic fields to less than 5 mG at the interaction region. All internal spectrometer components were also manufactured from nonmagnetic materials.

Experimental data acquisition. Naturally occurring magnesium has three stable isotopes, which occur with abundances of 79% (^{24}Mg), 10% (^{25}Mg), and 11% (^{26}Mg). Both ^{24}Mg and ^{25}Mg isotopes have zero nuclear spin, making them ideal for these studies since they have no hyperfine structure, as is found for ^{25}Mg. ^{24}Mg was hence chosen for this work as it has the greatest abundance. The ground state of ^{24}Mg is the $3\,^1S_0$ state, and the first dipole-allowed excited state is the $3\,^1P_1$ state with excitation energy of around 4.35 eV (the state chosen for these studies). There are three lower states between the $3\,^1P_1$ state and the $3\,^1S_0$ state, which are the $3\,^3P_{2,1,0}$ states, however, transitions to these states are not dipole allowed from either the $3\,^1S_0$ state or the $3\,^1P_1$ state, and so take no part in the laser-interaction process. As such, the interaction between the laser beam and magnesium atoms can be considered as an almost perfect two-level interaction. Further, since there are no hyperfine states in this isotope, the $3\,^1P_1$ state can be aligned with high purity by a linearly polarized laser beam.

Figure 3 shows a fluorescence measurement taken from laser excitation of the magnesium atoms as the laser beam was scanned in frequency. The largest signal occurs from the dominant isotope as expected. Under these experimental conditions the excitation energy of the ^{24}Mg $3\,^1P_1$ state is 1050810722 MHz, equivalent to a vacuum wavelength of 285.2963447 nm. The laser beam was hence set to this frequency throughout data acquisition, by operating a servocontrol system taken from the WSU wavelength meter.

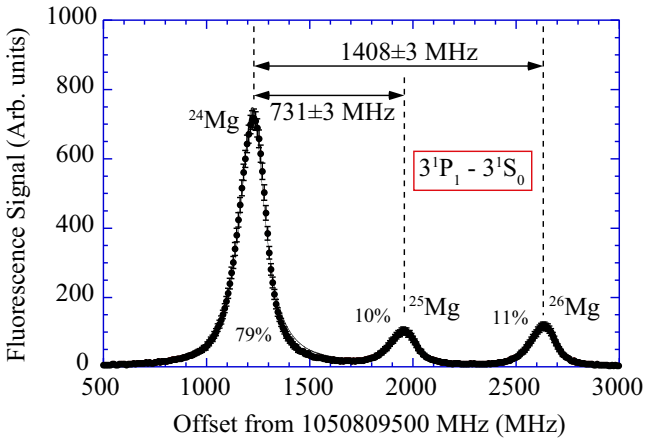

FIG. 3. Fluorescence excitation spectra observed using the UV photodiode, showing excitation of the different isotopes of magnesium by the laser beam. The spectrum is offset from 1050809500 MHz so that a comparison of the isotopic mass shifts in energy can be seen. The dominance of the ^{24}Mg isotope is clearly observed. These isotopes were selected for the superelastic studies discussed in this paper.

Once the laser beam was adjusted to excite ^{24}Mg atoms in the interaction region, the energies of the electron gun and analyzers were set to acquire an energy loss and gain spectrum. Figure 4 shows an example of these spectra taken with the laser beam on and off resonance. In this example the analyzer was set to a fixed energy of 35 eV and scattering angle of 45°, and the electron gun was scanned in energy through ±5 eV with respect to the elastic peak.

The open circles in Fig. 4 show the data when the laser beam is off resonance. There is hence no signal to the left of the elastic peak, which represents the region where electrons have gained energy from the interaction. The data to the right of the elastic peak correspond to inelastic scattering from magnesium, and this shows excitation of the $3\,^3P_{2,1,0}$ states (which could not be individually resolved) at 2.7 eV, as well as excitation of the $3\,^1P_1$ state at 4.35 eV. These nondipole-allowed triplet states

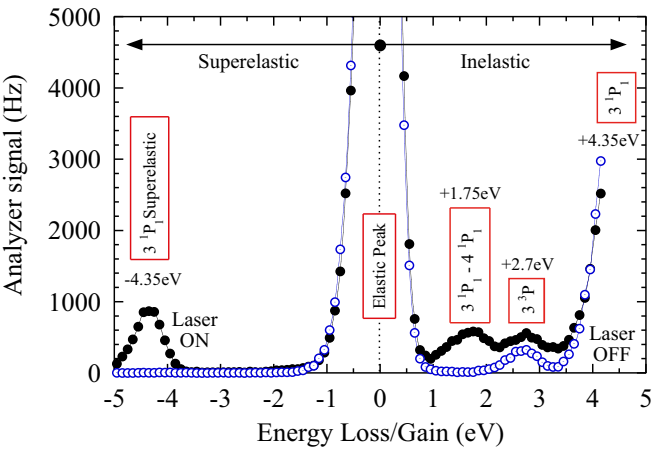

FIG. 4. Energy loss and gain spectrum from electron interaction with ^{24}Mg atoms in the interaction region, referenced to the position of the elastic peak.

are observed since the electron-impact collision allows them to be directly excited through exchange processes.

By contrast, when the laser beam was brought onto resonance with the $3\,^1P_1$ state, two new peaks emerged. These data are shown with the closed circles in Fig. 4. Superelastically scattered electrons are seen as a well-defined peak to the left of the elastic peak. This signal arises from the incident electrons interacting with laser-excited atoms so that they gain energy from the interaction, while deexciting the atoms back to the ground state. It is this signal that is used in the superelastic studies presented here. A new peak is also seen to the right of the elastic peak at 1.75 eV, which corresponds to incident electrons further exciting the laser-excited atoms in the $3\,^1P_1$ state to the $4\,^1P_1$ state (and to higher states). This peak in the inelastic spectrum only occurs when the laser is on resonance.

Measurements of P_ℓ and γ were hence carried out by setting the energy of the analyzers to a fixed value, and then adjusting the gun energy to be 4.35 eV lower than this energy. By blocking and unblocking the resonant laser beam, the signals from the analyzers would then vary from around 0 Hz (blocked) to that given by the superelastic scattering process (which depends upon the electron scattering angle and the polarization angle of the laser beam). For a given fixed scattering angle the half-wave plate was rotated through 360° so as to vary the polarization of the laser beam. Under normal conditions, this allows the ACPs to be determined by subtracting the on-resonance signal from that obtained when the laser is blocked. This method is well documented and was used in previous work from the University of Manchester [53–58].

This method of background subtraction could not be carried out for the present superelastic studies of magnesium, since it was found that fluorescence radiation from laser-excited atoms that passed into the analyzers would also produce an electron signal, since 285-nm light has sufficient energy to liberate photoelectrons from the molybdenum surfaces inside the analyzers. Different methods were attempted to reduce this unwanted background signal; however, it was not possible to eliminate the photoelectron signal entirely. It was therefore necessary to collect data both on and off resonance with the superelastic signal.

In practice it is difficult to quickly change the laser frequency to achieve this aim, and so a different technique was chosen to ascertain the contribution of photoelectrons to the analyzer count rates. The method adopted here was to initially set the gun energy to produce superelastically scattered electrons, and then quickly change this energy by 3 eV, so that superelastically scattered electrons could then not be observed. Changing the electron beam energy was straightforward to implement in the spectrometer, allowing the photoelectron signal to be determined independently of the superelastic signal.

Figure 5 shows an example of the signals obtained using this technique as the laser polarization vector rotated around the scattering plane. The "raw" analyzer signal is shown as open circles, whereas the signal with the gun detuned by 3 eV is shown as open diamonds (the photoelectron signal). The true superelastic signal is then determined by subtracting the photoelectron background signal from the raw signal, and this is shown as closed circles in Fig. 5. It can be seen that both the amplitude and the relative phase of the true signal differs

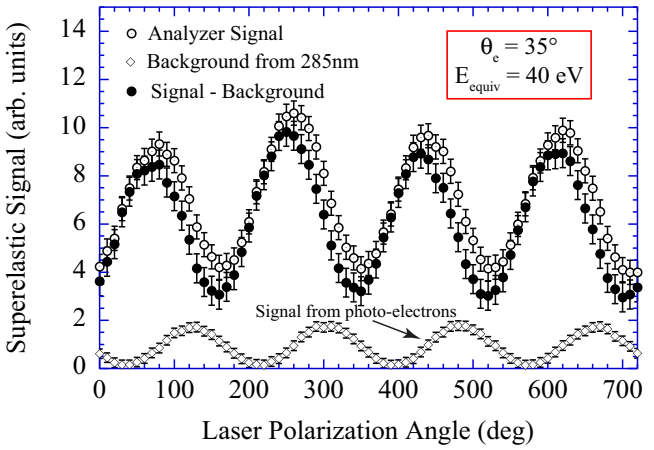

FIG. 5. Signal from the analyzer when the laser beam was on resonance with the atomic beam, as the half-wave plate was rotated through 360°. The raw superelastic signal is shown as open circles. The lower signal (shown as diamonds) was measured by adjusting the gun energy by 3 eV, so that there was no contribution from superelastic scattering. This signal arises from photoelectrons produced by fluorescence radiation striking surfaces inside the analyzer. The closed circles show the resulting superelastic signal when this background was subtracted from the raw signal.

from that of the raw signal. Since the amplitude variation of the superelastic signal is directly related to P_ℓ, and the phase angle is directly related to γ (see below), it is important to determine the true superelastic signal at each scattering angle to calculate the corresponding ACPs. This is particularly critical when the cross section is low, as the true signal from the electron collision may then be comparable to that from photoelectrons produced in the detectors.

IV. CONVERGENT CLOSE-COUPLING THEORY

The convergent close-coupling (CCC) theory was initially developed for the e-H collision system [61]. It was then extended to incorporate quasi-one-electron targets such as Na [62], two-electron targets such as He [63], and then quasi-two-electron targets such as Mg [64]. This nonrelativistic CCC theory has also been extended to light and heavy projectiles and molecular targets [65]. A relativistic implementation, necessary for heavy targets and highly charged ions, has also been developed [66].

Here we are interested in the e-Mg scattering system. The CCC method has already been extensively applied to this problem to study the $3\,^1P_1$ optical excitation function [67], compare with measurement of ACPs at 20 eV [9,10], resolve convergence problems at low energies [10], address discrepancy with experiment for the total ionization cross section [68], and for astrophysical modeling [69]. Consequently, we only give a brief overview of the essential theoretical concepts.

The target is treated as a two-valence electron atom with an inert Hartree-Fock core. The strong electron-electron correlation in the ground state requires a multiconfiguration treatment of the active electrons. Given the data is at energies well above the ionization threshold, a thorough representation of the target continuum is also required. The ACPs are essentially ratios of

scattering amplitude components, and as such are particularly sensitive to computational stability. As a consequence, a careful study of convergence, against both the target structure and the size of the close-coupling expansion, is required to achieve numerical stability.

In the present CCC calculations we begin by performing a self-consistent Hartree-Fock calculation to obtain the core orbitals. The CCC method relies on its convergence by utilization of a truncated complete Laguerre basis of size N_l and exponential fall-off λ_l for $l \leqslant l_{\text{top}}$. We set $l_{\text{top}} = 3$, and take $N_l = 20 - l$ with $\lambda_l = 2$, and diagonalize the frozen-core Hartree-Fock Hamiltonian of Mg^+ to generate one-electron orbitals. The resulting $1s$, $2s$, and $2p$ orbitals are not used, and we also drop the three highest-energy orbitals. An extensive multiconfiguration treatment of the target structure leads to a total of 513 target states upon the diagonalization of the Mg frozen-core Hamiltonian. These states are used in the close-coupling expansion to solve for the scattering amplitudes. Convergence with respect to the structure accuracy and Laguerre basis size has been checked with only the final 513 state results being presented. Relativistic CCC calculations were also attempted; however, relativistic effects were found to be negligible. We estimate an uncertainty of 5% at most scattering angles.

V. COMPARISON OF THEORY TO EXPERIMENT

As detailed in [55], the superelastic signal $Y_\theta(\varepsilon)$ for a scattering angle θ can be fitted to a function of the form

$$Y_\theta(\varepsilon) = A_\theta + B_\theta \cos^2(\varepsilon + C_\theta), \tag{3}$$

where ε is the laser polarization angle with respect to the direction of the incident electron beam, and A_θ, B_θ, C_θ are parameters that directly relate to P_ℓ and γ through the relationships

$$P_\ell(\theta) = \frac{B_\theta}{2A_\theta + B_\theta} \tag{4}$$

and

$$\gamma(\theta) = C_\theta + \theta + \frac{n\pi}{2}, \tag{5}$$

where n is an integer chosen to ensure $-\pi/2 \leqslant \gamma(\theta) \leqslant +\pi/2$.

Experiments were carried out using both analyzers, since each could access different parts of the scattering plane as described above. The analyzers were initially set to a given angle, and the electron gun and analyzer electrostatic lenses adjusted to produce superelastic signals from the interaction region when the laser was on resonance. Raw superelastic data were collected for a set time (typically 10–60 s) with the laser polarization angle varying from 0° (i.e., along the electron beam direction) to 720° in 10° steps, as in Fig. 5. The electron gun was then detuned by 3 eV, and the background signal obtained so that the true superelastic signal could be determined. Equations (4) and (5) were then fitted to the data using LABVIEW to determine P_ℓ and γ after each run. This procedure was repeated several times at each scattering angle, so that a statistically significant set of results could be obtained. The analyzers were then moved to new angles, and the procedure repeated until a complete set of parameters was obtained at a given energy $E_{\text{equiv.}}$. Four energies were adopted here, with $E_{\text{equiv}} = 35,\ 40,\ 45$, and 55 eV.

Figure 6 shows the results of this analysis for outgoing electron energies of 35 and 40 eV, and Fig. 7 shows the results for $E_{\text{equiv}} = 45$ and 55 eV. The experimental data were collected over scattering angles from $\theta_e = 25°$ to $\theta_e = 125°$, taken every 2.5°. The CCC calculation using 513 target states is also shown for direct comparison between experiment and theory.

At all energies the comparison between the calculated values of the alignment angle γ and experimental data is impressive, with the calculation closely emulating the results at all scattering angles. It should be noted that the apparent discontinuity in the data when γ passes through $\pm 90°$ [at around $\theta = 50°$ in Figs. 6(b) and 6(d)] is not real, since the P-state alignment angle is identical when $\gamma = 90°$ and $-90°$ (see Fig. 1).

Results for P_ℓ are less satisfactory at the lower energies adopted here, although the positions of the peaks and troughs in the data are predicted well by the model. At the highest energy $E_{\text{equiv.}} = 55$ eV there is good agreement both in position and magnitude of P_ℓ, with the P state being fully aligned at scattering angles $\theta > 100°$ where $P_\ell \approx 1.0$. As this energy decreases the agreement is less satisfactory, with the data showing an additional minimum at around $\theta = 120°$ that is only weakly predicted. It is interesting to note that the alignment angle γ is modeled well in this region, and so this additional structure in P_ℓ is likely to be due to small differences in the magnitude of the scattering amplitudes.

By contrast to the experimental data, the CCC theory consistently predicts P_ℓ to be near unity at the largest angles for all energies. This only agrees with experiment at the highest energy considered here, and there also exist some visible discrepancies at angles above $\theta = 80°$ for all energies. An extensive test of convergence of the CCC calculations was undertaken during this study as detailed above, and this indicated stability in the presented results. It would be helpful to have other computational approaches such as the R-matrix with the pseudostates (RMPS) model [2] applied to this problem, to allow additional comparisons to be made. Further experimental measurements of the angular momentum transferred to the atoms during the collision (i.e., the $L_\perp$ parameter) would also help to identify the cause of these differences, since for a fully coherent system $P_\ell^2 + L_\perp^2 = 1$. Additional experiments that determine $L_\perp$ are hence currently being considered, to explore this region further.

VI. SUMMARY AND CONCLUSIONS

In this paper the first superelastic scattering results from magnesium have been presented for alignment of the atoms by electron impact, as determined by the atomic collision parameters P_ℓ and γ. The results are presented over a range of equivalent energies from 35 to 55 eV. Data were obtained over a range of scattering angles from $\theta_e = 25°$ to 125°, allowing the variation in the parameters to be characterized in detail. The experimental results have been compared to a convergent close-coupling model, using 513 target states. The calculation accurately predicts the state alignment angle for all energies at

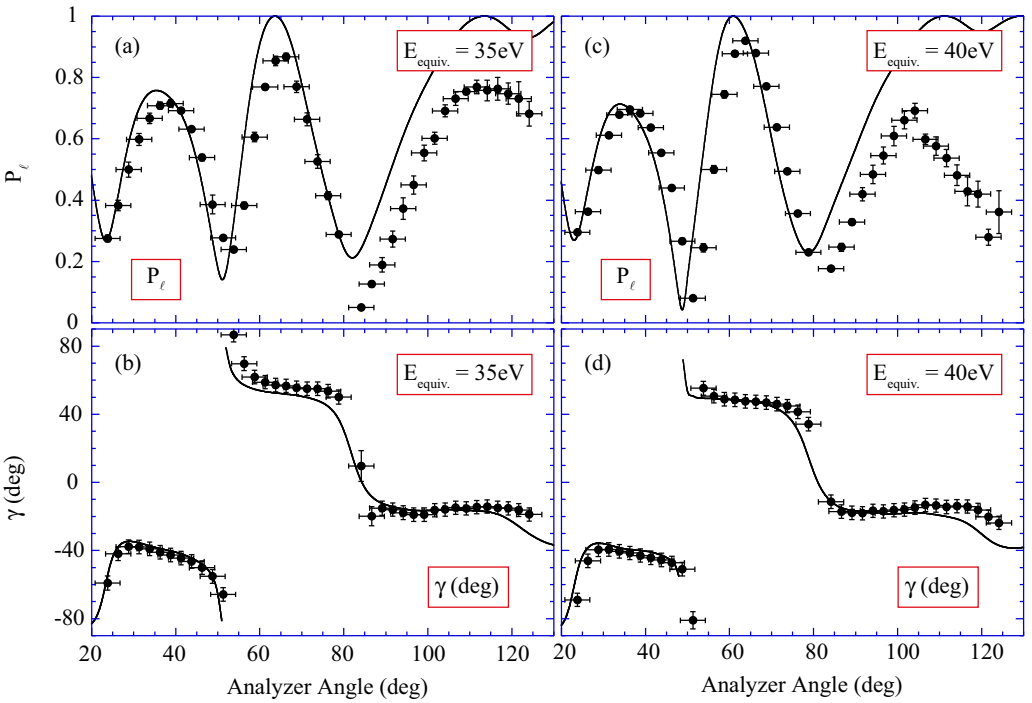

FIG. 6. Measurement of the (P_ℓ, γ) parameters for electron-impact excitation of the ground state of Mg to $3\,^1P_1$ using the superelastic technique for equivalent incident energies of 35 and 40 eV, compared to theoretical calculations using the CCC model with 513 target states (solid line).

all angles, and also accurately predicts the degree of alignment at the highest equivalent energy. For lower energies the data indicate that an additional minimum occurs in P_ℓ at high scattering angles that is not predicted by the CCC calculations; however, at smaller angles there is close agreement between the calculation and the data.

These experiments require high-intensity UV radiation at 285 nm, which has only recently become available using commercial high-resolution laser sources. The spectral resolution of these lasers allows individual isotopes to be preferentially excited in the experiments, so that depolarizing effects due to hyperfine structure can be completely eliminated. This is

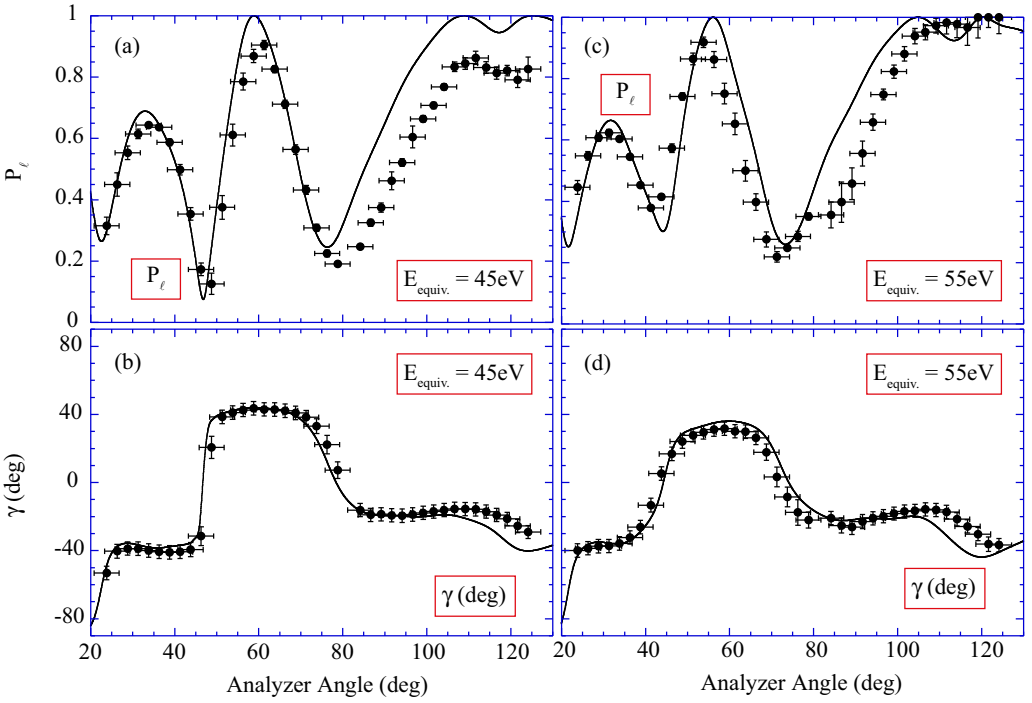

FIG. 7. Same as for Fig. 6, except for equivalent incident energies of 45 and 55 eV.

a considerable advantage compared to previous coincidence studies using alkali targets, since the results can be presented to high precision without the need to consider these depolarizing effects. In the present experiments the superelastic signals were relatively low at higher angles, and so extensive accumulation times were required to ensure accurate data were obtained in these regions. It was further found that fluorescence from the laser-atom interaction released photoelectrons from surfaces inside the spectrometer, and so the effect of these signals on the superelastic data had to be eliminated. This was accomplished by retuning the electron gun at each angle of the laser polarization vector, so that the photoelectron signal could be measured independently. The true superelastic signal was then calculated by subtracting the photoelectron signal from that of the raw signal.

To provide a complete description of the scattering process and contrast the results from theory with experiment, it is important to also measure the atomic collision parameter $L_\perp$, which defines the angular momentum transferred to the atom during the collision. This was not attempted in the current studies, and measurements of this parameter are now being considered for the near future.

ACKNOWLEDGMENTS

The Engineering and Physical Science Research Council (EPSRC) UK is thanked for providing a Ph.D. bursary for J.P., and for providing research Grant No. R120272. K.N. would like to thank the European union for a Marie Curie incoming international fellowship while in Manchester. We would also like to thank Dr. Alisdair MacPherson for assisting with the cw dye-laser system that was used here. Computational work was supported by resources provided by the Pawsey Supercomputing Centre with funding from the Australian Government and the Government of Western Australia, as well as the Australian Research Council.

[1] B. Bederson, Comments At. Mol. Phys. **1**, 41 (1969).
[2] B. Bederson, Comments At. Mol. Phys. **1**, 65 (1969).
[3] N. Andersen, K. Bartschat, and J. Kessler, *Polarization, Alignment and Orientation in Atomic Collisions* (Springer, Berlin, 2017).
[4] H. A. Yalim and A. Crowe, Turk. J. Phys. **26**, 219 (2002).
[5] M. L. Gradziel and R. W. O'Neill, J. Phys. B **37**, 1893 (2004).
[6] J. F. Williams and A. G. Mikosza, J. Phys. B **39**, 4113 (2006).
[7] D. Cvejanovic, D. T. McLaughlin, and A. Crowe, J. Phys. B **33**, 3013 (2000).
[8] L. Klosowski, M. Piwinski, D. Dziczek, K. Pleskacz, and S. Chwirot, Phys. Rev. A **80**, 062709 (2009).
[9] D. O. Brown, D. Cvejanovic, and A. CroweJ. Phys. B **36**, 3411 (2003).
[10] D. O. Brown, A. Crowe, D. V. Fursa, I. Bray, and K. Bartschat, J. Phys. B **38**, 4123 (2005).
[11] D. Dyl, D. Dziczek, M. Piwinski, M. Gradziel, R. Srivastava, R. S. Dygdala, and S. Chwirot, J. Phys. B **32**, 837 (1999).
[12] S. Milisavljevic, D. Sevic, V. Pejcev, D. M. Filipovic, and B. P. Marinkovic, J. Phys. B **37**, 3571 (2004).
[13] J. F. Williams, D. Cvejanovic, S. Samarin, L. Pravica, S. Napier, and A. Sergeant, J. Phys.: Conf. Ser. **80**, 012023 (2007).
[14] S. Kawazoe, T. Kai, R. K. Chauhan, R. Srivastava, and S. Nakazaki, J. Phys. B **39**, 493 (2006).
[15] O. Zatsarinny, K. Bartschat, L. Bandurina, and S. Gedeon, J. Phys. B **40**, 4023 (2007).
[16] R. K. Chauhan, R. Srivastava, and A. D. Stauffer, J. Phys. B **38**, 2385 (2005).
[17] L. R. Hargreaves, C. Campbell, M. A. Khakoo, J. W. McConkey, O. Zatsarinny, K. Bartschat, A. D. Stauffer, and R. P. McEachran, Phys. Rev. A **87**, 022711 (2013).
[18] L. R. Hargreaves, R. Wright, M. A. Khakoo, O. Zatsarinny, K. Bartschat, Dipti, R. Srivastava, and A. D. Stauffer, J. Phys. B **48**, 185201 (2015).
[19] L. R. Hargreaves, C. Campbell, M. A. Khakoo, O. Zatsarinny, and K. Bartschat, Phys. Rev. A **85**, 050701(R) (2012).
[20] M. Piwinski, D. Dziczek, L. Klosowski, and S. Chwirot, Eur. Phys. J. Spec. Top. **222**, 2273 (2013).
[21] M. Piwinski, L. Klosowski, D. Dziczek, S. Chwirot, T. Das, R. Srivastava, A. D. Stauffer, C. J. Bostock, D. V. Fursa, and I. Bray, Phys. Rev. A **86**, 052706 (2012).
[22] M. Piwinski, L. Klosowski, D. Dziczek, S. Chwirot, D. V. Fursa, and I. Bray, Phys. Rev. A **91**, 062704 (2015).
[23] M. Piwinski, L. Klosowski, S. Chwirot, D. V. Fursa, I. Bray, T. Das, and R. Srivastava, J. Phys. B **51**, 085002 (2018).
[24] M. Piwinski, D. Dziczek, R. Srivastava, M. Gradziel, and S. Chwirot, J. Phys. B **35**, 3821 (2002).
[25] M. Piwinski, D. Dziczek, L. Klosowski, R. Srivastava, and S. Chwirot, J. Phys. B. **39**, 1945 (2006).
[26] M. J. Berrington, C. J. Bostock, D. V. Fursa, I. Bray, R. P. McEachran, and A. D. Stauffer, Phys. Rev. A **85**, 042708 (2012).
[27] C. Herting, G. F. Hanne, K. Bartschat, K. Muktavat, R. Srivastava, and A. D. Stauffer, J. Phys. B **36**, 3877 (2003).
[28] G. Aussendorf, F. Juttemann, K. Muktavat, L. Sharma, R. Srivastava, A. D. Stauffer, K. Bartschat, D. V Fursa, I. Bray, and G. F. Hanne, J. Phys. B **39**, 2403 (2006).
[29] G. Aussendorf, F. Juttemann, K. Muktavat, L. Sharma, R. Srivastava, A. D. Stauffer, K. Bartschat, D. V. Fursa, I. Bray, and G. F. Hanne, J. Phys. B **39**, 4435 (2006).
[30] C. Herting and G. F. Hanne, J. Phys. B **35**, L91(2002).
[31] C. Herting, G. F. Hanne, K. Bartschat, A. N. Grum-Grzhimailo, K. Muktavat, R. Srivastava, and A. D. Stauffer, J. Phys. B **35**, 4439 (2002).
[32] F. Juttemann, G. F. Hanne, O. Zatsarinny, and K. Bartschat, Phys. Rev. A **79**, 042712 (2009).
[33] F. Juttemann, G. F. Hanne, O. Zatsarinny, K. Bartschat, R. Srivastava, R. K. Gangwar, and A. D. Stauffer, Phys. Rev. A **81**, 012705 (2010).
[34] N. Andersen and K. Bartschat, Adv. At. Mol. Phys. **36**, 1 (1996).
[35] I. V. Hertel and W. Stoll, J. Phys. B: At. Mol. Phys. **7**, 570 (1974).
[36] I. V. Hertel and W. Stoll, Adv. At. Mol. Phys. **13**, 113 (1978).
[37] R. E. Scholten, G. F. Shen, and P. J. O. Teubner, J. Phys. B **26**, 987 (1993).

[38] K. A. Stockman, V. Karaganov, I. Bray, and P. J. O. Teubner, J. Phys. B **31**, L867 (1998).
[39] B. V. Hall, Y. Shen, A. J. Murray, M. C. Standage, W. R. MacGillivray, and I. Bray, J. Phys. B **37**, 1113 (2004).
[40] V. Karaganov, I. Bray, and P. J. O. Teubner, J. Phys. B **31**, L187 (1998).
[41] D. S. Slaughter, V. Karaganov, M. J. Brunger, P. J. O. Teubner, and I. Bray, Phys. Rev. A **75**, 062717 (2007).
[42] P. V. Johnson, B. Eves, P. W. Zetner, D. Fursa, and I. Bray, Phys. Rev. A **59**, 439 (1999).
[43] J. D. Hein, C. Ududec, D. K. Sasaki, and P. W. Zetner, J. Phys. B. **43**, 185206 (2010).
[44] J. D. Hein, P. W. Zetner, C. J. Bostock, D. V. Fursa, I. Bray, T. Das, and R. Srivastava, J. Phys. B **45**, 115202 (2012).
[45] P. V. Johnson and P. W. Zetner, J. Phys. B **38**, 2793 (2005).
[46] P. V. Johnson, C. Spanu, Y. Li, and P. W. Zetner, J. Phys. B **33**, 5367 (2000).
[47] P. V. Johnson, C. Spanu, and P. W. Zetner, J. Phys. B **34**, 4311 (2001).
[48] Y. Li and P. W. Zetner, Phys. Rev. A **49**, 950 (1994).
[49] P. W. Zetner and P. V. Johnson, J. Phys. B **39**, 455 (2006).
[50] R. Srivastava and A. D. Strauffer, Phys. Rev. A **71**, 052715 (2005).
[51] P. W. Zetner, P. V. Johnson, Y. Li, G. Csanak, R. E. H. Clark, and J. Abdallah, J. Phys. B **34**, 1619 (2001).
[52] A. J. Murray and D. Cvejanovic, J. Phys. B **36**, 4889 (2003).
[53] M. Hussey, A. J. Murray, W. R. MacGillivray, and G. C. King, Phys. Rev. Lett. **99**, 133202 (2007).
[54] M. Hussey, A. J. Murray, W. R. MacGillivray, and G. C. King, J. Phys. B **41**, 055202 (2008).
[55] A. J. Murray, W. R. MacGillivray, and M. Hussey, Phys. Rev. A **77**, 013409 (2008).
[56] A. Knight-Percival, S. Jhumka, M. Hussey, and A. J. Murray, J. Phys. B **44**, 105203 (2011).
[57] M. Hussey, S. Jhumka, and A. J. Murray, Phys. Rev. A **86**, 042705 (2012).
[58] S. Jhumka, K. L. Nixon, M. Hussey, and A. J. Murray, Phys. Rev. A **87**, 052714 (2013).
[59] A. J. Murray, B. C. H. Turton, and F. H. Read, Rev. Sci. Instrum. **63**, 3346 (1992).
[60] J. N. H. Brunt, G. C. King, and F. H. Read, J. Phys. B **10**, 1289 (1977).
[61] I. Bray and A. T. Stelbovics, Phys. Rev. A **46**, 6995 (1992).
[62] I. Bray, Phys. Rev. A **49**, 1066 (1994).
[63] D. V. Fursa and I. Bray, Phys. Rev. A **52**, 1279 (1994).
[64] D. V. Fursa and I. Bray, J. Phys. B **30**, 5895 (1997).
[65] I. Bray, A. B. Abdurakhmanov, J. J. Bailey, A. W. Bray, D. V. Fursa, A. S. Kadyrov, C. M. Rawlins, J. S. Savage, A. T. Stelbovics, and M. C. Zammit, J. Phys. B **50**, 202001 (2017).
[66] C. J. Bostock, D. V. Fursa, and I. Bray, Phys. Rev. A **82**, 022713 (2010).
[67] D. V. Fursa and I. Bray, Phys. Rev. A **63**, 032708 (2001).
[68] I. Bray, K. McNamara, and D. V. Fursa, Phys. Rev. A **92**, 022705 (2015).
[69] P. S. Barklem, Y. Osorio, D. V. Fursa, I. Bray, O. Zatsarinny, K. Bartschat, and A. Jerkstrand, Astron. Astrophys. **606**, A11 (2017).